MOLECULAR AND CELLULAR BIOLOGY, Sept. 1993, p. 5814–5828
0270-7306/93/095814-15$02.00/0

Vol. 13, No. 9

eps15, A Novel Tyrosine Kinase Substrate, Exhibits Transforming Activity

FRANCESCA FAZIOLI,[1] LILIANA MINICHIELLO,[1] BRONA MAŤOŠKOVÁ,[2] WILLIAM T. WONG,[1] AND PIER PAOLO DI FIORE[1]*

Laboratory of Cellular and Molecular Biology, National Cancer Institute,[1] and Laboratory of Cellular Development and Oncology, National Institute of Dental Research,[2] Bethesda, Maryland 20892

Received 10 May 1993/Returned for modification 25 May 1993/Accepted 21 June 1993

An expression cloning method which allows direct isolation of cDNAs encoding substrates for tyrosine kinases was applied to the study of the epidermal growth factor (EGF) receptor (EGFR) signaling pathway. A previously undescribed cDNA was isolated and designated *eps*15. The structural features of the predicted *eps*15 gene product allow its subdivision into three domains. Domain I contains signatures of a regulatory domain, including a candidate tyrosine phosphorylation site and EF-hand-type calcium-binding domains. Domain II presents the characteristic heptad repeats of coiled-coil rod-like proteins, and domain III displays a repeated aspartic acid-proline-phenylalanine motif similar to a consensus sequence of several methylases. Antibodies specific for the *eps*15 gene product recognize two proteins: a major species of 142 kDa and a minor component of 155 kDa, both of which are phosphorylated on tyrosine following EGFR activation by EGF in vivo. EGFR is also able to directly phosphorylate the *eps*15 product in vitro. In addition, phosphorylation of the *eps*15 gene product in vivo is relatively receptor specific, since the *erb*B-2 kinase phosphorylates it very inefficiently. Finally, overexpression of *eps*15 is sufficient to transform NIH 3T3 cells, thus suggesting that the *eps*15 gene product is involved in the regulation of mitogenic signals.

The mechanisms by which tyrosine kinase (TK) growth factor receptors (RTKs) transduce mitogenic stimuli into target cells are still poorly understood. It is widely accepted that most, if not all, of the signal transduction repertoire is initially activated by tyrosine-specific phosphorylation events of intracellular molecules by RTKs (for review, see references 1 and 60). Accordingly, a number of proteins have been identified which are phosphorylated on tyrosine after activation of RTKs and are thought to be intermediates of the signaling cascade (1, 60). These includes the γ isozyme of phospholipase C (PLC-γ) (42, 44, 62); the GTPase-activating protein *ras*-GAP (16, 28, 30, 47) and at least two proteins associated with it, p62 and p190 (16, 56, 66); the p85 subunit of phosphatidylinositol 3-kinase (PtdIns-3K) (8, 17, 29, 49, 52, 57, 61); several intracellular *src*-like kinases (23, 35); and the *shc* gene product (50).

Although efforts have been directed at establishing the biological relevance for mitogenic signaling of these substrates, studies have not yet produced a coherent picture. The case of PLC-γ is paradigmatic. PLC-γ catalyzes the breakdown of phosphatidylinositol 1,3-bisphosphate, and phosphorylation/activation of PLC-γ by several RTKs results in increased PIP_2 hydrolysis, which in turn correlates with cell proliferation (reviewed in references 41 and 64). Microinjection of purified PLC-γ has been reported to cause DNA synthesis and morphological transformation of NIH 3T3 cells (58). However, genetically engineered overexpression of PLC-γ did not result in enhanced mitogenic response to platelet-derived growth factor (PDGF), despite increased PIP_2 turnover (43). Similarly, structure-function studies of RTKs indicated that PLC-γ binding/phosphorylation is dispensable for the transduction of mitogenic signals (46, 51).

It is likewise unclear whether PtdIns-3K activity is required for mitogenesis. Transforming $p60^{v\text{-}src}$ mutants invariably show associated PtdIns-3K activity, suggesting that this enzyme may be necessary for the growth-promoting action of the v-Src protein (22). However, tyrosine mutations in the interkinase domain of the α PDGF receptor abrogated receptor-associated PtdIns-3K activity without affecting mitogenic or chemiotactic signaling (67). A possible unifying hypothesis to reconcile these observations is that at least some known second messengers are part of redundant mitogenic pathways. Accordingly, they would be individually dispensable as mitogenic effectors. If this were true, it is reasonable to think that additional mitogenic pathways exist, which await isolation and characterization.

We are interested in the mechanisms of signal transduction by the epidermal growth factor (EGF) receptor (EGFR) and the related *erb*B-2/*neu* receptor. Both of these receptors elicit sizable mitogenic response in NIH 3T3 cells (reviewed in references 10 and 13); however, it is not clear whether a significant fraction of these signals is routed through known effector pathways. Both EGFR and *erb*B-2 kinases, in fact, induce very low stoichiometry of PLC-γ phosphorylation, and only when activated at supraphysiological levels in NIH 3T3 cells (20). Similarly, they are inefficient at phosphorylating *ras*-GAP (20). In comparison, PDGF receptors, expressed in the same cells at physiological levels, can trigger phosphorylation of these two molecules with high stoichiometry (20). Moreover, in the NIH 3T3 system, following activation of the EGFR or *erb*B-2 kinase, we detected little activation of PtdIns-3K and low levels of *raf* tyrosine phosphorylation (19, 20). These results suggest that other, yet uncharacterized, pathways might be activated by EGFR and *erb*B-2 in NIH 3T3 fibroblasts.

We endeavored, therefore, to characterize additional substrates for the EGFR kinase. We developed an expression cloning strategy for cDNAs encoding EGFR substrates (18, 21). In this paper, we report the isolation and characterization of the *eps*15 (EGFR pathway substrate clone no. 15) cDNA. *eps*15 encodes a 142-kDa protein that is phosphory-

* Corresponding author.

lated on tyrosine residues following EGFR activation. In addition, p142^{eps15} is phosphorylated much more efficiently following activation of the EGFR compared with the *erb*B-2 kinase, suggesting that it might be part of a relatively EGFR-specific signaling mechanism. Finally overexpression of p142^{eps15} causes transformation of NIH 3T3 cells, thus raising the possibility that this molecule is involved in the control of cell proliferation.

MATERIALS AND METHODS

Isolation and characterization of the *eps*15 cDNA. The previously described antibodies (Ab) 450 and 451 (18) were used to screen a commercial (Clontech) λgt11 library from NIH 3T3 cells. The screening method is reported in detail elsewhere (21). Briefly, 10^6 recombinant plaques were initially screened with a 1:200 dilution of each Ab in TTBS (0.05% Tween, 20 mM Tris-HCl [pH 7.5], 150 mM NaCl) containing 1% bovine serum albumin. Detection was carried out with a goat anti-rabbit Ab conjugated to alkaline phosphatase, by using a commercial kit (Picoblue; Stratagene) as specified by the manufacturer. One of the positive phages, pl 15, was plaque purified, and its ~1.8-kbp insert, excised from the λgt11 recombinant with *Eco*RI, was subcloned in the *Eco*RI site of pBluescript.

To obtain the full-length *eps*15 cDNA, we screened a mouse keratinocyte cDNA library (45), using the pl 15 insert as a probe, by standard procedures (53). The DNA sequence was determined by the dideoxy termination method on both strands of the *eps*15 cDNA, using a commercial kit (Sequenase). The GenBank and EMBL data bases were screened with the BLAST program (2). Signatures of the predicted protein sequence were identified by the PROSITE program (3).

Northern blot analysis on poly(A)$^+$ RNA prepared from NIH 3T3 cells was performed, with the pl 15 insert as a probe, as described previously (53).

Cell lines. NIH 3T3 fibroblasts transfected with eukaryotic expression vectors for EGFR (11) and for the chimeric receptors EGFR/*erb*B-2 (20, 39), EGFR/*erb*B-2^{COOH} (14, 15), EGFR/*erb*B-2^{TK} (15), and EGFR/*erb*B-2^{TK-1} (9, 55) have been described previously. The chimeric vectors used in the experiments shown contained a transmembrane region from gp185^{erbB-2}, but similar results were obtained with chimerae bearing the EGFR transmembrane. All of the cell lines were cultivated in Dulbecco's modified Eagle's medium supplemented with 10% (vol/vol) calf serum.

The BALB/MK cell line (63) was cultivated in low-calcium Dulbecco's modified Eagle's medium supplemented with 10% dialyzed fetal calf serum and 4 ng of EGF per ml, as described previously (63).

DNA synthesis was monitored by [^{3}H]thymidine incorporation as described previously (20).

Transfection studies and transformation assays. DNA transfection of NIH 3T3 cells was performed by the calcium phosphate precipitation technique, as modified by Wigler et al. (65). Transformed foci were scored at 3 weeks. Transforming efficiency was calculated in focus-forming units (FFU) per picomole of added DNA after normalization for the efficiency of colony formation in parallel dishes subjected to selection in G418-containing medium (59). Cells expressing the neomycin resistance gene were selected for their ability to form colonies in the presence of a G418-containing medium (59).

For the analysis of the transformed phenotype (see Fig. 12), foci of morphological transformation were picked, by cloning cylinders, from plates transfected with pCEV-*eps*15 which had not been exposed to G418-containing medium. Morphologically normal areas (flat areas) were also picked from the same plates. Both foci and flat areas were then subjected to G418 selection, and the growth of killer-resistant populations was monitored. Foci that arose from a cell that received transfected DNA grew vigorously and reached confluence rapidly (quick selection). For the flat areas, in contrast, killer-resistant populations developed over a much longer period, since they originated from rare transfected flat cells which were picked in the surface of a cloning cylinder (the frequency of transfection is estimated to be $\sim 10^{-2}$ cells for NIH 3T3). Similarly, pseudofoci (foci of spontaneous transformation, not dependent on DNA transfection) developed into killer-resistant populations at the same rate as the flat areas did, since it is unlikely (frequency $\sim 10^{-2}$) that a pseudofocus originates from a transfected cell. Only populations displaying the quick-selection phenotype were used for further studies.

Anchorage-independent growth was measured in soft agar, as described previously (11, 12).

Protein studies. Polyclonal antibodies specific for the *eps*15 gene product were generated against a recombinant TrpE fusion protein in the pATH 11 expression vector (33). To this end, the open reading frame (ORF) of pl 15, encompassed between two *Eco*RI sites, was cloned in frame in the *Eco*RI site of the pATH 11 bacterial expression vector. The recombinant fusion protein was expressed by induction with tryptophan and indoleacrylic acid (33), gel purified, and used to immunize New Zealand rabbits.

The GST-eps15 fusion protein was obtained by cloning the ORF of the pCEV-*eps*15 cDNA into the pGEX-KG expression vector (a kind gift of T. Ishibashi), a derivative of the pGEX-2T vector (Pharmacia). Recombinant polymerase chain reaction (PCR) was used to obtain a fragment of the *eps*15 cDNA encompassing the sequence from the gene encoding amino acid 2 to the natural stop codon located after amino acid 897. PCR primers were designed to yield the *eps*15 cDNA fragment flanked by unique *Xba*I and *Xho*I sites, at the 5′ and 3′ ends of the PCR product, respectively. After digestion with *Xba*I and *Xho*I, the fragment was cloned in frame between the homologous sites of pGEX-KG. Induction and purification of the GST-eps15 fusion protein were carried out as specified by the manufacturer. Where indicated, digestion with thrombin (Sigma) was carried out by incubating 1 μg of fusion protein with 150 ng of thrombin in 50 μl of a buffer containing 150 mM NaCl, 50 mM Tris-HCl (pH 8.0), and 2.5 mM $CaCl_2$.

Phosphotyrosine (pTyr)-containing proteins were detected with a commercially available anti-pTyr monoclonal antibody (Upstate Biotechnology). Specificity of detection for anti-pTyr was controlled as described previously (55).

Immunoprecipitation, immunoblotting, and coimmunoprecipitation experiments were performed as previously described (18, 20, 21). Typically, we used 100 μg of total cellular proteins for direct immunoblot analysis and 2 mg of total cellular proteins for immunoprecipitation and immunoblotting experiments. Except when otherwise indicated, treatment with EGF in vivo was performed at a concentration of 17 nM EGF for 5 to 10 min at 37°C, after 12 to 16 h of serum starvation.

^{125}I-EGF saturation binding assays were performed at a final EGF concentration of 167 nM (1 μg/ml; cold/hot EGF ratio, 3:1) for 6 h at 4°C, as described previously (11, 55).

For the in vitro transcription and translation experiments, 5 μg of linearized pCEV-*eps*15 was incubated for 1 h at 37°C

in a buffer containing 40 mM Tris HCl (pH 7.5), 10 mM $MgCl_2$, 2 mM spermidine, 10 mM NaCl, 10 mM dithiothreitol, 120 U of RNasin (Promega), 0.5 mM deoxynucleoside triphosphates, and 40 U of Sp6 polymerase (Boehringer Mannheim), in a final reaction volume of 100 μl. After 1 h, an additional 120 U of RNasin and 40 U of Sp6 polymerase were added and the reaction was continued for another 1 h. After treatment with 40 U of RNase-free DNase (Boehringer Mannheim), samples were extracted with phenol-chloroform and precipitated out of 0.15 M NaCl–70% ethanol. Dried pellets were resuspended in RNase-free water and stored at −70°C. For the in vitro translation, 1 μg of the in vitro-transcribed RNA was incubated at 30°C for 1 h in a final reaction volume of 50 μl containing 35 μl of nuclease-treated rabbit reticulocyte lysate (Promega), 15 U of RNasin, 20 mM complete amino acid mixture (Promega), and 15 μCi of L-[^{35}S]methionine (specific activity, 1,200 Ci/mmol; Amersham). Reactions were stopped by the addition of Laemmli buffer and directly analyzed by sodium dodecyl sulfate-polyacrylamide gel electrophoresis (SDS-PAGE).

Immunocomplex kinase assays were performed essentially as previously described (55). Briefly, EGFRs were immunoprecipitated from equal amounts of lysates of NIH EGFR cells with a monoclonal Ab directed against the extracellular domain of the EGFR (Ab-1; Oncogene Science). Immunoprecipitates, recovered with protein G-agarose, were resuspended in 30 μl of HNTG (0.1% Triton X-100, 20 mM HEPES [*N*-2-hydroxyethylpiperazine-*N*′-2-ethanesulfonic acid; pH 7.5], 150 mM NaCl, 10% glycerol) supplemented with 15 mM $MgCl_2$, 15 mM $MnCl_2$, and 40 μM unlabeled ATP and incubated at 4°C for 10 min. This step was designed to obtain prephosphorylation of the EGFR with unlabeled ATP and to prevent competition between the EGFR and the substrate(s) in the subsequent phosphorylation step in the presence of labeled ATP. Beads were extensively washed in HNTG buffer and resuspended in 30 μl of HNTG containing 15 mM $MgCl_2$, 15 mM $MnCl_2$, 20 μCi of [γ-^{32}P]ATP (specific activity, 3,000 Ci/mmol; New England Nuclear), and 1 μg of purified GST-*eps*15 and incubated at 4°C for 10 min. Supernatants from the kinase reactions were then processed either by immunoprecipitation with anti-*eps*15 or by affinity chromatography on glutathione-agarose, as indicated.

Subcellular fractionation. NIH EGFR cells, treated as described in the legend to Fig. 8, were washed three times with cold phosphate-buffered saline containing 0.5 μM sodium orthovanadate and scraped into a hypotonic lysis buffer, HBL [10 mM Tris (pH 7.4), 10 mM NaCl, 3 mM $MgCl_2$, 1 mM EDTA, 1 mM ethylene glycol-bis(β-aminoethyl ether)-*N*,*N*,*N*′,*N*′-tetraacetic acid (EGTA), 1 mM sodium orthovanadate, 10 mM sodium PP_i, 1 mM phenylmethylsulfonyl fluoride, 10 μg of aprotinin per ml, 10 mM NaF]. The cells were incubated on ice for 10 min and Dounce homogenized (40 strokes) with a tight-fitting pestle. The homogenate was designated as the total fraction. The total fraction was further separated into nuclear and postnuclear fractions by low-speed centrifugation (375 × *g*) for 5 min. The pellet (nuclear fraction) was further washed five times with HLB containing 0.1% Nonidet P-40 to remove membrane and/or cytosolic contamination. The soluble, postnuclear fraction was centrifuged again at low speed for 10 min to remove nuclear contamination and then subjected to high-speed centrifugation (150,000 × *g*) for 30 min. The pellet (membrane fraction) was washed with HBL and centrifuged again to recover the final membrane fraction. The supernatant (cytosolic fraction) was centrifuged again at high speed to remove membrane contamination, and the supernatant was defined as the cytosolic fraction. All fractions were adjusted to 50 mM Tris (pH 7.4), 100 mM NaCl, 1 mM EDTA, 1 mM EGTA, 3 mM $MgCl_2$, 0.5% deoxycholate, 0.1% SDS, 0.2% Nonidet P-40, 10 μg of aprotinin per ml, 1 mM phenylmethylsulfonyl fluoride, 10 mM sodium PP_i, 10 mM sodium orthovanadate, and 50 mM NaF and then centrifuged at 12,000 × *g* for 15 min to remove insoluble material. All the procedures were performed on ice. Each fraction was assayed for the presence of lactate dehydrogenase (cytosolic marker) and alkaline phosphodiesterase (membrane marker).

Nucleotide sequence accession number. The sequence reported in this paper has been entered in the GenBank data base and assigned accession number L21768.

RESULTS

Isolation of the *eps*15 cDNA. We have previously described two polyclonal sera (sera 450 and 451) which recognize several proteins that are tyrosine phosphorylated upon EGF stimulation of NIH 3T3 fibroblasts overexpressing the EGFR (NIH EGFR cells) (18). These sera were used to immunologically screen a λgt11 cDNA library prepared from NIH 3T3 fibroblasts (21). Analysis of 10^6 recombinant phages yielded several positive plaques; one of these clones (pl 15) contained an insert of 1,838 bp (Fig. 1A) whose sequence did not match sequences present in the GenBank or EMBL data bank. The sequence of pl 15 predicted an ORF which started in the expected frame with the β-galactosidase portion of λgt11 but contained neither an initiation nor a stop codon (Fig. 1A). Thus, pl 15 represented a partial cDNA encoding a previously undescribed protein which we designated eps15.

To obtain a full-length clone of eps15, we screened a mouse keratinocytes cDNA library (45) with pl 15 as a probe. Several cDNAs were isolated, and the longest one (pCEV-*eps*15) was sequenced. The complete sequence of pCEV-*eps*15 is shown in Fig. 1B. The 3,074-bp sequence contained a stop codon at position 2802 to 2804, followed by 270 bp of 3′ untranslated sequence containing a putative polyadenylation site (AATTAAA, starting at position 3014). The first in-frame ATG (position 111 to 113) conformed to Kozak's rules for translational initiation (34) and was preceded by 110 bp of 5′ untranslated sequences.

The sequence of pCEV-*eps*15 did not contain an in-frame stop codon preceding the putative ATG, thus raising the possibility that it does not represent a full-length cDNA. To elucidate this issue, we studied the expression of mRNA encoded by the *eps*15 gene by performing Northern (RNA) blot analysis of poly(A)$^+$ RNA extracted from NIH 3T3 cells, with the pl 15 insert as a probe. Two major bands of ~3.3 and ~6.0 kb were detected (Fig. 1, inset). The size of the smaller band is in agreement with that of the pCEV-*eps*15 cDNA clone, whereas the 6.0-kb band may be a partially processed precursor or an alternatively spliced form. These results, together with those obtained in in vitro transcription-translation and in in vivo expression experiments (see below) indicate that pCEV-*eps*15 makes up the entire coding region for *eps*15.

***eps*15 gene product.** The amino acid sequence deduced from the single *eps*15 ORF (Fig. 2A) predicts an 897-amino-acid protein with a calculated molecular mass of ~98 kDa. The features of the predicted polypeptide suggest that it can be divided into at least three structural domains (Fig. 2A). Domain I (spanning amino acids 9 to 314) consists of three

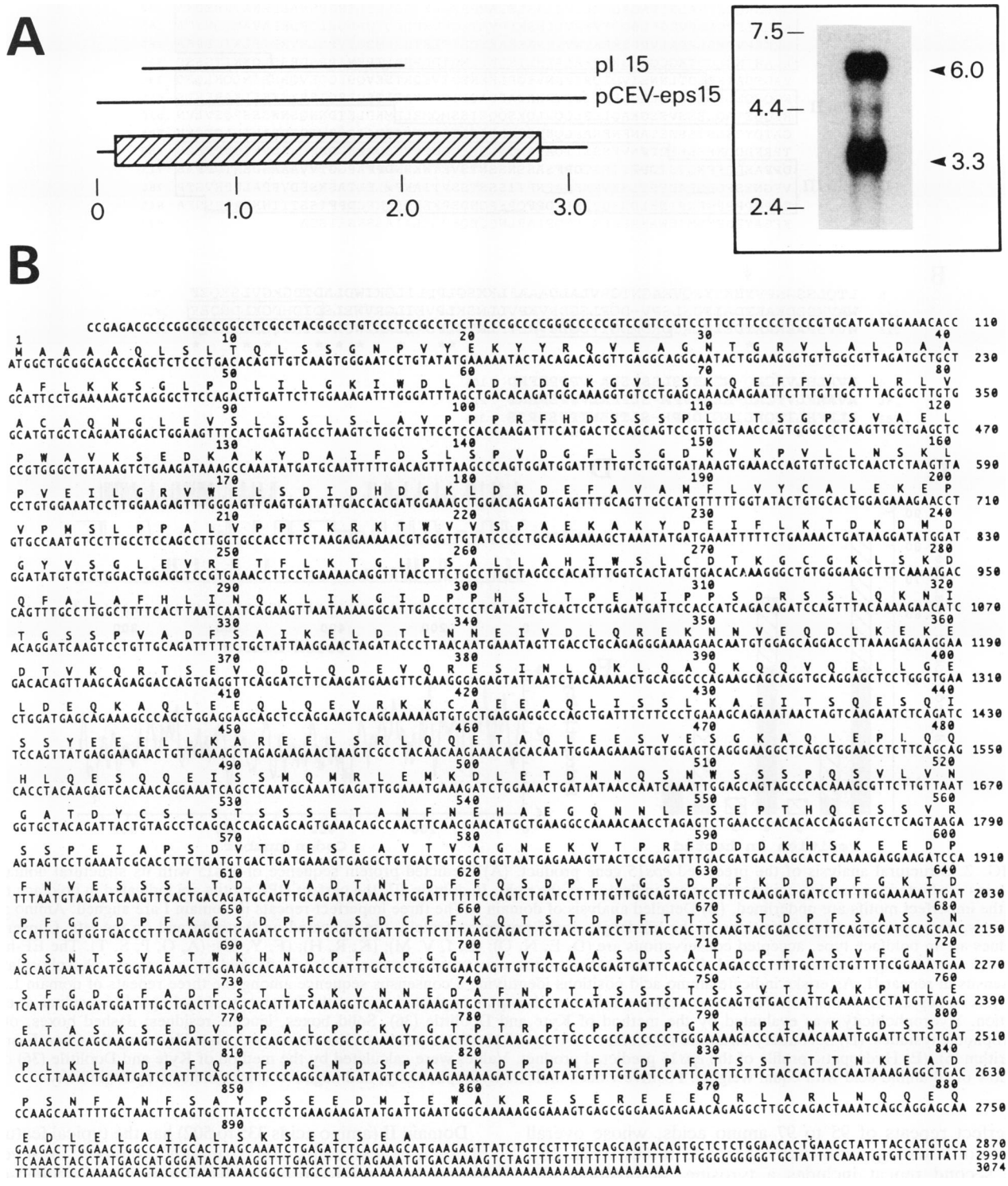

FIG. 1. Structure and sequence of the *eps*15 cDNA. (A) The structures of the pl 15 and pCEV-*eps*15 cDNAs are depicted, in comparison with a schematic representation of the encoded mRNA. The ORF is indicated by a dashed box. Positions are indicated in kilobases. (B) Nucleotide sequence and predicted amino acid sequence of *eps*15 cDNA. Nucleotide positions are indicated on the right. Amino acid positions are indicated above. (Inset) Expression of *eps*15 mRNA. Poly(A)$^+$ RNA (5 μg) from NIH 3T3 cells was fractionated on an agarose-formaldehyde gel and analyzed by Northern blot with a nick-translated pl 15 probe. Molecular size markers are shown in kilobases.

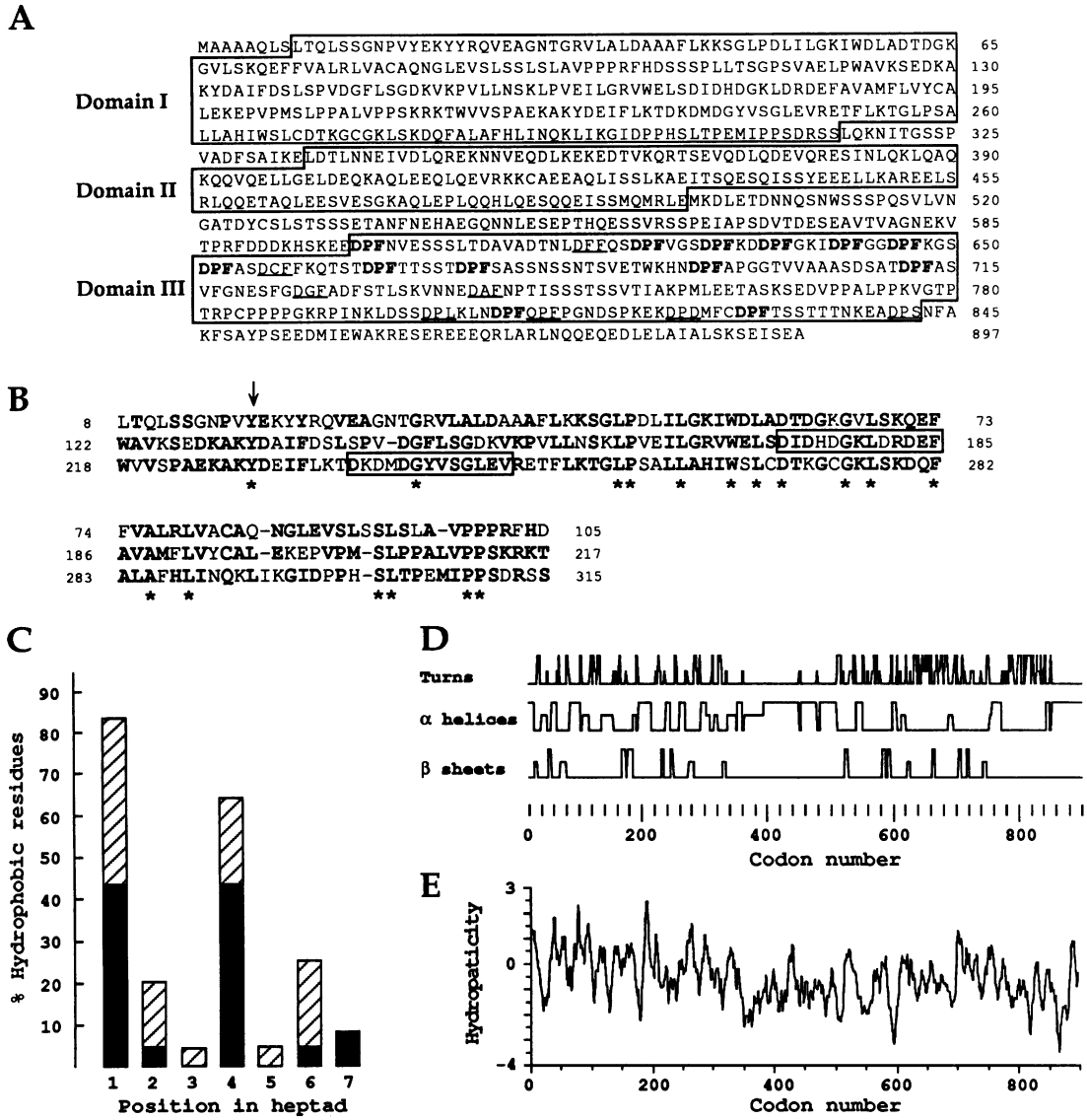

FIG. 2. Structural analysis of the predicted *eps*15 gene product. (A) Predicted protein sequence of eps15 with its structural domains. Domains are boxed, and amino acid positions are indicated on the right. In domain III, the perfect DPF motifs are indicated in boldface type and the imperfect motifs are underlined. (B) Detailed analysis of domain I. The three imperfect repeats in domain I are aligned. Amino acid positions, corresponding to the positions in the full-length eps15 predicted protein, are indicated on the right and on the left. Conserved residues are in boldface type; accepted conservations are (D, E, N, Q); (L, I, V, M); (K, R, H); (F, Y, W); (A, G, P, S, T). The EF-hand type calcium-binding domains are boxed. The arrow indicates the conserved tyrosine, which is flanked by a tyrosine phosphorylation consensus in repeat II. Asterisks indicate amino acid positions identifying a consensus sequence among the three repeats of domain I. (C) Analysis of heptads in domain II. The amino acid position in each heptad is plotted against the frequency of hydrophobic residues at each position. Hydrophobicity was evaluated by the method of Kyte and Doolittle (36). Solid boxes, leucine residues; dashed boxes, other hydrophobic residues. (D) Secondary-structure prediction of the *eps*15 predicted product. Scores were calculated by using the Chou-Fasman algorithm (6). (E) Hydropatic profile of the *eps*15 predicted product. Values were calculated by the method of Kyte and Doolittle (36) on a window of 10 amino acid with equal weights. Positive values indicate hydrophobicity, and negative values indicate hydrophilicity.

imperfect repeats of 95 to 97 amino acids, whose overall degree of homology with each other is 55 to 60% (Fig. 2B). The second repeat includes a tyrosine, at position 132, flanked by a consensus sequence for putative tyrosine phosphorylation sites (3, 27). This tyrosine residue is conserved in the first and third repeats of domain I, although it lacks the flanking motif. The second and third repeats also contain consensus sequences for EF-hand calcium-binding domains (3, 26) at positions 173 to 185 and 236 to 248, respectively (Fig. 2B).

Domain II (amino acids 335 to 502) has the typical features of an α-helical coiled-coil structure, common to several cytoskeleton-related proteins. The formation of a coiled-coil α-helix requires heptad repeats, in which the first and fourth positions usually contain hydrophobic amino acid residues (40). Domain II of eps15 is composed of 24 contiguous heptads whose positions 1 and 4 are markedly biased in favor of apolar amino acids, in particular leucine (Fig. 2C). In addition, domain II contains only two glycines and one proline (1.8% of the total residues, as opposed to 11.8% in

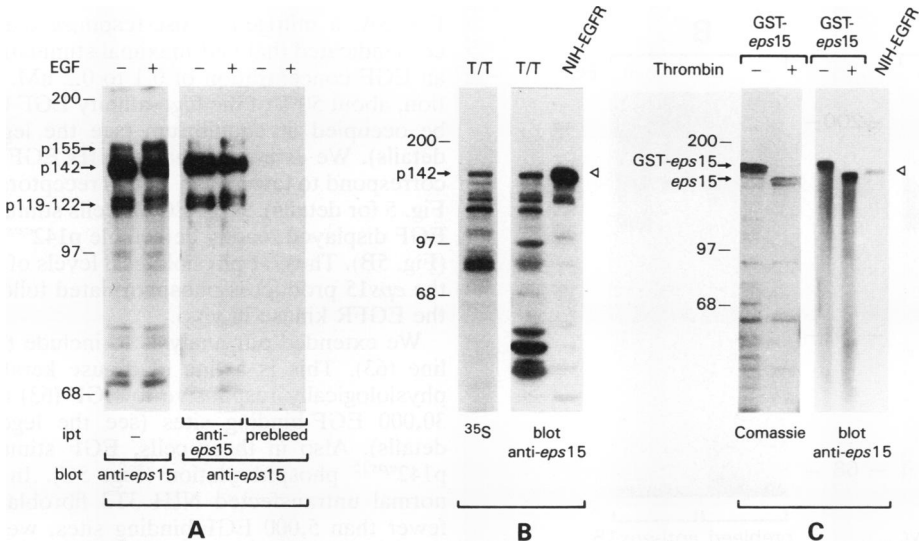

FIG. 3. Identification of the *eps*15 gene product(s). (A) Total-cell lysates obtained from NIH EGFR cells (11, 20) were analyzed by immunoprecipitation and/or immunoblot with the anti-*eps*15 Ab or the corresponding preimmune serum (prebleed). When indicated (+), intact cells were treated with 17 nM EGF for 10 min at 37°C ipt, immunoprecipitation; blot, immunoblot. (B) The pCEV-*eps*15 cDNA was transcribed and translated in vitro, as described in Materials and Methods, in the presence of L-[^{35}S]methionine. The product of the in vitro transcription/translation (T/T) was then fractionated by SDS-PAGE, blotted onto Immobilon membranes, and analyzed by autoradiography (left panel [indicated by ^{35}S]); we also loaded in a parallel lane 100 μg of total cellular proteins extracted from NIH EGFR cells. After autoradiography, the same Immobilon filter was immunostained with the anti-*eps*15 Ab (right panel, indicated as blot anti-*eps*15) and detection was carried out with ^{125}I-protein A. Autoradiography was then performed by shielding the low-energy β-emission of L-[^{35}S]methionine with layers of aluminum foil. Under these conditions, we were able to detect only the high-energy γ-emission of ^{125}I-protein A. (C [left panel, Coomassie blue]) The GST-eps15 fusion protein (1 μg), obtained as described in Materials and Methods, was either digested with thrombin or mock treated and then analyzed by SDS-PAGE followed by Coomassie blue staining. (C [right panel, blot anti-*eps*15]) The GST-eps15 fusion protein (100 ng) was either digested with thrombin or mock treated and then analyzed by SDS-PAGE followed by immunoblotting with the anti-eps15 Ab. Total cellular lysate (100 μg) from NIH EGFR cells was also loaded on the gel to identify authentic p142^{eps15}. The arrows in panels B and C indicate the position of authentic p142^{eps15}. Molecular mass markers are indicated in kilodaltons.

the entire eps15), which are both strong α-helix breakers. Secondary-structure prediction (Fig. 2D) indicated that this region has the potential to form an α-helix.

Domain III (amino acid 598 to 842; Fig. 2A) is characterized by the repetition of a 3-amino-acid motif, aspartic acid-proline-phenylalanine (DPF repeat); we identified 13 perfect DPFs and 8 imperfect repeats (DXF, DPX, and XPF). A hydropaticity plot of eps15 (Fig. 2E) did not reveal any long stretch of hydrophobic amino acids that might qualify as a transmembrane domain or a signal peptide. No SH2 or SH3 domains, which are characteristic signatures of many RTK substrates (reviewed in reference 32), were identified.

Identification of the *eps*15 gene product. To characterize the *eps*15 gene product, we expressed the ORF from the pl 15 clone in the pATH 11 (33) bacterial expression vector (data not shown) and raised polyclonal antibodies against the recombinant fusion protein. The anti-eps15 serum recognized in NIH EGFR cells (11) a doublet of 142 and 155 kDa (Fig. 3A), the 142-kDa band being the major component, which was not detected with the corresponding preimmune serum (Fig. 3A). A second doublet of much lower intensity, migrating as 119 and 122 kDa, was also specifically recognized by the anti-*eps*15 serum but not by the preimmune serum (Fig. 3A). The major band (p142) recognized by the anti-eps15 Ab was significantly larger than the predicted *eps*15 gene product (~98 kDa). This difference was not due to N-linked glycosylation, since no differences in the electrophoretic mobility of eps15 were detectable after tunycamicin treatment (data not shown).

To investigate the nature of the discrepancy between the electrophoretic mobility of the *eps*15 gene product and its predicted molecular mass, we performed in vitro transcription and translation of the pCEV-*eps*15 cDNA. As shown in Fig. 3B (left panel), the ^{35}S-labeled product of the transcription-translation experiment contained a major species of 140 to 145 kDa, in addition to several other smaller products. We interpreted the 140- to 145-kDa band as the primary translational product of the pCEV-*eps*15 cDNA and the smaller bands as degradation products or as the results of the translation of incompletely elongated mRNAs. To confirm this, we immunostained the same blot with the anti-*eps*15 Ab. As shown in Fig. 3B (right panel), the 140- to 145-kDa band was promptly recognized under these conditions. In addition, this band comigrated with authentic p142^{eps15} present in an NIH EGFR lysate (Fig. 3B, right panel).

The possibility also had to be considered that we underestimated the predicted molecular mass of the *eps*15 gene product as a result of an error in the assignment of the stop codon. To address this, we obtained by PCR an *eps*15 cDNA fragment encompassing exclusively the sequence from the gene encoding amino acid 2 to the predicted stop codon following amino acid 897 and expressed this fragment as a fusion protein with the glutathione *S*-transferase (GST) in the pGEX vector. As shown in Fig. 3C (left panel), the purified GST-eps15 fusion protein exhibited a molecular mass of ~160 kDa. Cleavage with thrombin, which releases the GST portion, yielded a ~140-kDa band which reacted promptly with the anti-eps15 Ab and migrated similarly to authentic p142^{eps15} (Fig. 3C). On the basis of all this evidence, we concluded that p142 is the primary translational product of the *eps*15 cDNA and that the discrepancy be-

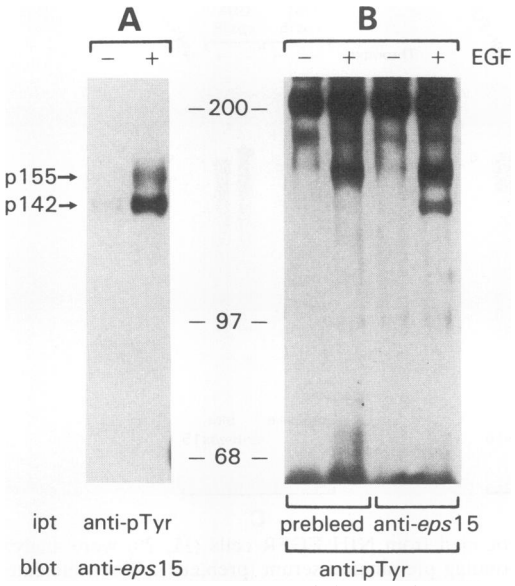

FIG. 4. Tyrosine phosphorylation of the *eps*15 gene product(s) following activation of the EGFR in vivo. NIH EGFR cells were either mock treated (lanes −) or treated with EGF (lanes +), (100 ng/ml; 17 nM) for 10 min at 37°C, and total cellular lysates were prepared as described in Materials and Methods. (A) Total cellular proteins (2 mg) were immunoprecipitated with the anti-pTyr Ab and analyzed in immunoblot with anti-eps15 Ab. (B) Total cellular proteins (2 mg) were immunoprecipitated with either the anti-eps15 or with the corresponding preimmune serum (prebleed) and analyzed in immunoblot with the anti-pTyr Ab. Molecular mass markers are indicated in kilodaltons.

tween the actual and predicted size of the *eps*15 gene product should be ascribed either to abnormalities in its gel migration or to putative posttranslational modifications that also occur in a reticulocytes lysate and/or in bacteria.

Tyrosine phosphorylation of the *eps*15 product in vivo and in vitro. To investigate the state of tyrosine phosphorylation of the *eps*15 gene product following EGFR activation, lysates were prepared from NIH EGFR cells, before and after in vivo EGF treatment, and analyzed by sequential immunoprecipitation and immunoblotting with anti-pTyr and anti-eps15 Abs. As shown in Fig. 4A, both p142^{eps15} and p155^{eps15} were phosphorylated in vivo on tyrosine following EGFR activation.

Anti-pTyr recovery of the *eps*15 product might be due to direct recognition of phosphotyrosyl residues or to association with other pTyr-containing proteins. To distinguish between these possibilities, we performed immunoprecipitation experiments with anti-eps15 followed by immunoblot with anti-pTyr. As shown in Fig. 4B, pTyr-containing p142^{eps15} was readily detectable in cell lysates obtained from NIH EGFR cells triggered with EGF. Under these conditions, tyrosine-phosphorylated p155^{eps15} was not easily detectable, probably because of the presence of a superimposed background band (Fig. 4B). All these results clearly establish that eps15 is tyrosine phosphorylated following EGFR activation.

We next analyzed whether the *eps*15 product is a physiological substrate in the EGFR-activated pathway. To do this, we used conditions of EGF stimulation able to elicit a sizable mitogenic signal but under which only a few thousands EGFRs were stimulated in NIH EGFR cells. As shown in Fig. 5A, a mitogenic dose-response curve in NIH EGFR cells indicated that half-maximal stimulation was obtained at an EGF concentration of 0.1 to 0.2 nM. At this concentration, about 50% of the high-affinity EGF-binding sites would be occupied at equilibrium (see the legend to Fig. 5 for details). We estimated that in NIH EGFR cells, this would correspond to fewer than 10,000 receptors (see the legend to Fig. 5 for details). NIH-EGFR cells stimulated with 0.17 nM EGF displayed readily detectable p142^{eps15} phosphorylation (Fig. 5B). Thus, at physiological levels of ligand stimulation, the *eps*15 product is phosphorylated following activation of the EGFR kinase in vivo.

We extended our analysis to include the BALB/MK cell line (63). This is a line of mouse keratinocytes which is physiologically responsive to EGF (63) and displays about 30,000 EGF-binding sites (see the legend to Fig. 5 for details). Also in these cells, EGF stimulation resulted in p142^{eps15} phosphorylation (Fig. 5C). In addition, even in normal untransfected NIH 3T3 fibroblasts, which exhibit fewer than 5,000 EGF-binding sites, we were able to evidence EGF-induced phosphorylation of the *eps*15 gene product (Fig. 5D).

To demonstrate that p142^{eps15} can be directly phosphorylated by the EGFR, we performed immunocomplex kinase assays in which EGFRs were immunoprecipitated from NIH EGFR cells and challenged with the purified GST-eps15 fusion protein in the presence of [γ-^{32}P]ATP as a phosphate donor. Under these conditions, ^{32}P incorporation was promptly detected in the GST-eps15 fusion protein whereas immunocomplexes obtained with an irrelevant monoclonal Ab exhibit considerably less ability to phosphorylate the fusion protein (Fig. 6). In addition, thrombin cleavage of the ^{32}P-containing GST-eps15 fusion protein yielded ^{32}P-containing authentic p142^{eps15}, thus showing that phosphorylation was carried out on the eps15 portion and not on the GST moiety (Fig. 6B).

Stoichiometry of phosphorylation in vivo and subcellular localization of eps15. We estimated the percentage of eps15 molecules phosphorylated in vivo, following activation of the EGFR. To do this, we initially determined the optimal conditions for eps15 phosphorylation in vivo. EGF induced maximal eps15 phosphorylation at a concentration of 17 nM (Fig. 5; data not shown); we therefore measured eps15 phosphorylation following treatment of NIH EGFR cells with 17 nM EGF as a function of time. As shown in Fig. 7A, eps15 phosphorylation was half-maximal after 15 s of stimulation and reached a plateau at 5 min. Therefore, we measured the stoichiometry of eps15 phosphorylation in vivo after 5 min of 17 nM EGF treatment. To this end, cell lysates from EGF-treated NIH EGFR cells were subjected to three sequential cycles of immunoprecipitation with anti-pTyr and the immunoprecipitates were analyzed in immunoblot with an anti-eps15 Ab (Fig. 7B). Aliquots of the supernatant from the immunoprecipitation reaction and of the total starting material were also analyzed in immunoblots (Fig. 7B). After autoradiography, the signals were quantitated in a phosphoimager scanner and the stoichiometry of in vivo phosphorylation was calculated after correction for the amount of material loaded (see the legend to Fig. 7 for details). We estimated that ~30% of the total eps15 pool was phosphorylated, under our conditions of analysis. Of note, we have reported previously that the stoichiometry of in vivo phosphorylation of PLC-γ in EGF-treated NIH EGFR cells under similar conditions is about 1% of the total PLC-γ pool (20).

We next determined the subcellular localization of the

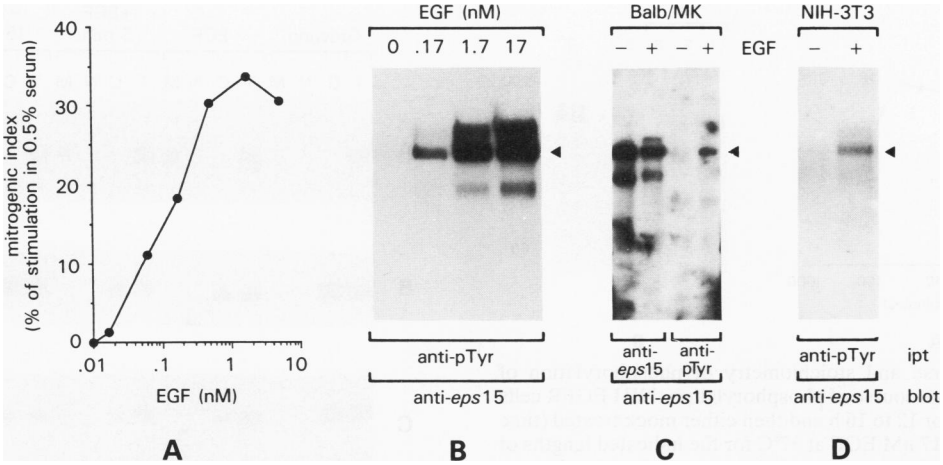

FIG. 5. Tyrosine phosphorylation of the *eps*15 gene product(s) in vivo at physiological levels of EGFR activation. (A) NIH EGFR cells were analyzed for their mitogenic responsiveness to increasing concentrations of EGF by [^{3}H]thymidine incorporation. The 50% effective dose for mitogenic response was 0.1 to 0.2 nM (about 1 ng/ml). The NIH EGFR cell line used in this experiment exhibited about 4×10^5 EGFRs per cell, as determined by ^{125}I-EGF saturation-binding assays (see Fig. 10). This particular NIH EGFR transfectant was completely characterized in terms of its EGF-binding abilities (9) and found to exhibit two classes of binding sites with K_ds in the range of 10^{-10} M (high affinity) and 10^{-8} M (low affinity), respectively. High-affinity binding sites made up about 5% of the total EGF-binding sites (9). On the basis of these values, we calculated that at an EGF concentration of 1 ng/ml (0.17 nM), fewer than 10,000 EGF-binding sites would be occupied at equilibrium. (B) NIH EGFR cells were either mock treated (lane 0) or treated with increasing concentrations of EGF for 10 min at 37°C. Total cellular proteins (2 mg) were immunoprecipitated with the anti-pTyr Ab and analyzed by immunoblot with the anti-eps15 Ab. Autoradiographic signals were quantitated by a phosphoimager scanner and yielded the following values (in arbitrary units): no EGF treatment, 1 U; 0.17 nM (1 ng/ml) EGF, 5.0 U; 1.7 nM (10 ng/ml) EGF, 21.8 U; 17 nM (100 ng/ml) EGF, 31.1 U. (C) BALB/MK mouse keratinocytes were either mock treated (lanes −) or treated with 17 nM EGF (lanes +) for 10 min at 37°C. Total cellular proteins (2 mg) were immunoprecipitated with either the anti-eps15 Ab or the anti-pTyr Ab and analyzed by immunoblot with the anti-eps15 Ab. ^{125}I-EGF-binding assays of this cell line revealed about 30,000 EGF-binding sites. (D) Normal untransfected NIH 3T3 mouse fibroblasts were either mock treated (lane −) or treated with 17 nM EGF (lane +) for 10 min at 37°C. Total cellular proteins (2 mg) were immunoprecipitated with the anti-pTyr Ab and analyzed by immunoblot with the anti-eps15 Ab. ^{125}I-EGF-binding assays of this cell line revealed about 3,000 to 5,000 EGF-binding sites. The arrowheads in panels B to D indicate the *eps*15 gene products.

*eps*15 gene product. To this end, NIH EGFR lysates were fractionated into cytosolic, nuclear, and membrane fractions, as described in Materials and Methods. The purity of individual fractions was assayed with specific markers. As shown in Fig. 8A and 8B, immunoblots with anti-PDGF receptor or anti-PLC-γ Abs revealed that these proteins were localized almost exclusively in the membrane and cytosolic fractions, respectively, as expected. In addition, assays of lactate dehydrogenase (cytosolic marker) and alkaline phosphodiesterase (membrane marker) enzymatic activities indicated that each of the analyzed fractions was more than 90% pure (see Materials and Methods for details). Aliquots of each fractions, representative of the same number of cells, were then analyzed in immunoblot with the anti-eps15 Ab. As shown in Fig. 8C, in resting serum-starved NIH EGFR cells, eps15 was localized to the cytosolic fraction. Subcellular localization did not appear to change appreciably after stimulation with EGF (5 and 15 min at a concentration of 17 nM) or in cells continuously grown in the presence of calf serum (Fig. 8C).

Specificity of eps15 phosphorylation. We have previously shown that EGFR and the highly related gp185$^{erbB\text{-}2}$ receptor deliver their signals into the cell through pathways which are at least partially distinct (9, 11, 12, 15, 55). Accordingly, qualitative and quantitative differences are detectable in the patterns of intracellular proteins which are phosphorylated on tyrosine on activation of the EGFR or *erb*B-2 kinases (20). However, when known RTKs substrates, including PLC-γ, *ras*-GAP, the p85 subunit of PtdIns-3K, and *raf* (19, 20), were analyzed, no differences could be detected be-

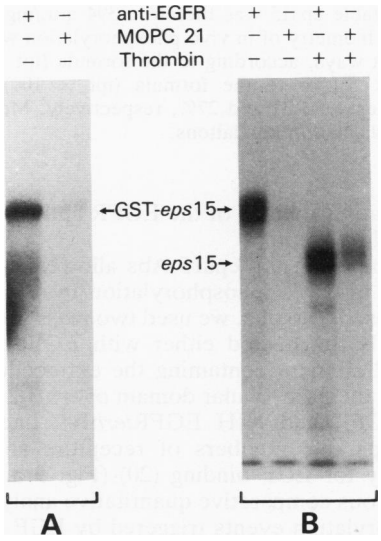

FIG. 6. In vitro tyrosine phosphorylation of bacterially expressed *eps*15 by EGFR. Immunocomplex kinase assay. Purified GST-eps15 fusion protein (1 μg) was subjected to phosphorylation by the EGFR under the conditions of an immunocomplex kinase assay, as described in Materials and Methods. Phosphorylated GST-eps15 was recovered either by affinity chromatography on glutathione-agarose (A) or with the anti-eps15 Ab (B) and analyzed by SDS-PAGE and autoradiography. Controls were performed by generating immunocomplex with the irrelevant monoclonal Ab MOPC21. Where indicated, the GST-eps15 fusion protein was digested with thrombin after the immunoprecipitation with the anti-eps15 Ab.

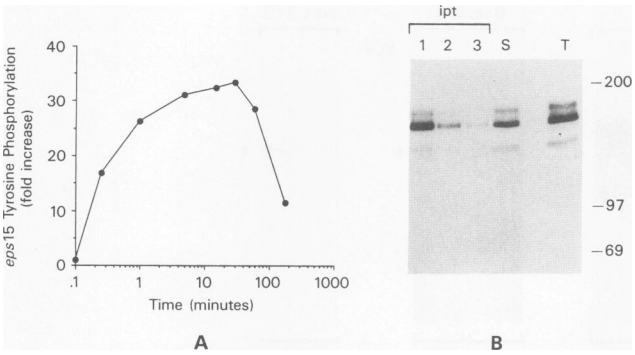

FIG. 7. Time course and stoichiometry of phosphorylation of eps15 in vivo. (A) Time course of phosphorylation. NIH EGFR cells were serum starved for 12 to 16 h and then either mock treated (time zero) or treated with 17 nM EGF at 37°C for the indicated lengths of time. Total cellular proteins were immunoprecipitated with the anti-pTyr Ab and detected in immunoblot with the anti-eps15 Ab. The intensity of signals was analyzed in a phosphoimager scanner and converted into fold increase with respect to the signal detected at time zero (assumed as an intensity of 1). (B) Stoichiometry of in vivo phosphorylation. NIH EGFR cells were treated with 17 nM EGF for 5 min at 37°C. Total cellular proteins (1 mg) were then immunoprecipitated three times with the anti-pTyr Ab (lanes ipt 1, 2, and 3), with immunocomplexes recovered after each immunoprecipitation. Immunoprecipitates were analyzed in immunoblot with the anti-eps15 Ab. The supernatant of the immunoprecipitation reaction (indicated as S, one-fifth of the total supernatant, corresponding to 200 μg of initial material) and an aliquot of the total cellular proteins (indicated as T, 200 μg of proteins) were also analyzed. Autoradiographic signals were quantified in a phosphoimager scanner and yielded the following values (expressed as arbitrary units [a.u.], representing the integrated volume of the band): ipt first cycle, 246 a.u.; ipt second cycle, 99 a.u.; ipt third cycle, 49 a.u.; supernatant (S), 176 a.u.; total (T), 293 a.u. The total anti-pTyr immunoprecipitable eps15 was therefore 394 a.u./mg of total proteins. The stoichiometry of in vivo phosphorylation was calculated in two different ways, according to the formula (ipt × 100)/[ipt + (supernatant × 5)] or to the formula (ipt × 100)/(total × 5); calculated values were 31 and 27%, respectively. Molecular mass markers are indicated in kilodaltons.

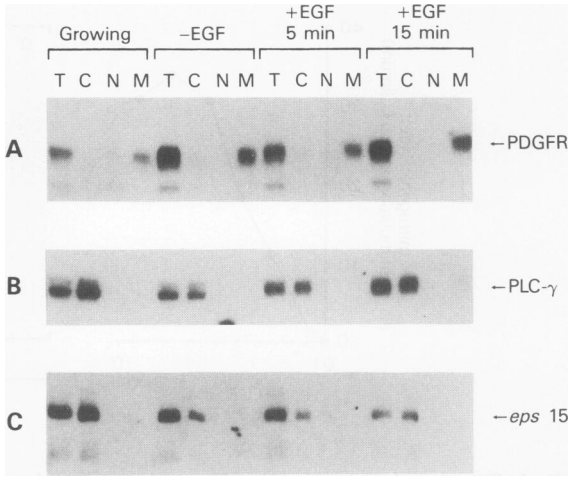

FIG. 8. Subcellular localization of the *eps*15 gene product. NIH EGFR cells were either starved in serum-free medium for 12 to 16 h or grown in the continuous presence of 10% calf serum (lanes Growing). Starved cells were then either mock treated (lanes −EGF) or treated with 17 nM EGF for 5 (lanes +EGF 5 min) or 15 (lanes +EGF 15 min) at 37°C. Subcellular fractions were obtained as described in Materials and Methods and are identified as C (cytosolic fraction), N (nuclear fraction), and M (membrane fraction). Aliquots of each fraction or of the total cellular lysate (T), representative of the same number of cells (5×10^5), were then analyzed by immunoblot with anti-PDGFR (A), anti PLC-γ (B) and anti-eps15 (C) Abs. Molecular mass markers are indicated in kilodaltons.

tween the relative abilities of the EGFR and *erb*B-2 kinases to phosphorylate them.

The availability of anti-eps15 Abs allowed us to test the specificity of p142^{eps15} phosphorylation by the EGFR and *erb*B-2 kinases. To do this, we used two mass populations of NIH 3T3 cells transfected either with EGFR or with an EGFR/*erb*B-2 chimera containing the extracellular domain of EGFR and the intracellular domain of *erb*B-2 (20, 37–39). The NIH EGFR and NIH EGFR/*erb*B-2 lines used expressed comparable numbers of receptors and exhibited similar affinity for EGF binding (20) (Fig. 9 and 10), thus allowing rigorous comparative quantitative analysis of the in vivo phosphorylation events triggered by EGF stimulation. As shown in Fig. 9A, EGF treatment of NIH EGFR/*erb*B-2 cells resulted in little if any tyrosine phosphorylation of p142^{eps15}, although it induced readily detectable autophosphorylation of the chimeric receptor (Fig. 9B) and phosphorylation of a number of other intracellular proteins (Fig. 9B). Conversely, EGF stimulation of NIH EGFR promptly triggered p142^{eps15} tyrosine phosphorylation (Fig. 9A). The differential response of NIH EGFR and NIH EGFR/*erb*B-2 could not be ascribed to intrinsic differences in the two cell lines, since PDGF stimulation was able to elicit p142^{eps15} phosphorylation in both of them (Fig. 9A). In addition, several other kinases, including insulin receptor, fibroblast growth factor receptor (stimulated by basic fibroblast growth factor) and colony-stimulating factor type 1 CSF-1 receptor were much less efficient than EGFR at phosphorylating eps15 in vivo (data not shown). We concluded, therefore, that tyrosine phosphorylation of p142^{eps15} is relatively receptor specific.

Mapping of the region responsible for differential tyrosine phosphorylation of eps15 by the EGFR and *erb*B-2 kinase. We next used a panel of cDNAs encoding chimeric molecules between EGFR and *erb*B-2 to map the region(s) of these receptors responsible for the differential phosphorylation of eps15. The products of the chimerae used are depicted in Fig. 10A. They were engineered by substituting coding domains of gp185^{erbB-2} for the corresponding regions of the EGFR and have been previously described and characterized (11, 14, 15, 55).

For the experiments shown here, we selected NIH 3T3 transfectants expressing comparable number of EGF-binding sites: about 4×10^5 to 5×10^5, as assessed by ^{125}I-EGF saturation binding (Fig. 10B). The wild-type EGFR and all the chimeric receptors exhibited comparable kinase activity in vivo, as evidenced by similar levels of autophosphorylation and ability to phosphorylate PLC-γ, following EGF exposure (data not shown) (9, 11, 14, 15, 20, 39, 55).

When the ability of the chimeric receptors to phosphorylate the *eps*15 gene product was analyzed, we noticed that an EGFR/*erb*B-2^{COOH} chimera, in which the carboxy-terminal (COOH) domain of gp185^{erbB-2} was substituted for the COOH domain of EGFR, was able to phosphorylate eps15 comparably to the wild-type EGFR (Fig. 11A). Conversely, the substitution of the TK region of gp185^{erbB-2} into EGFR (EGFR/*erb*B-2^{TK}) yielded a molecule which was severely impaired in its ability to phosphorylate eps15 (Fig. 11A). Further mapping showed that the substitution of the first

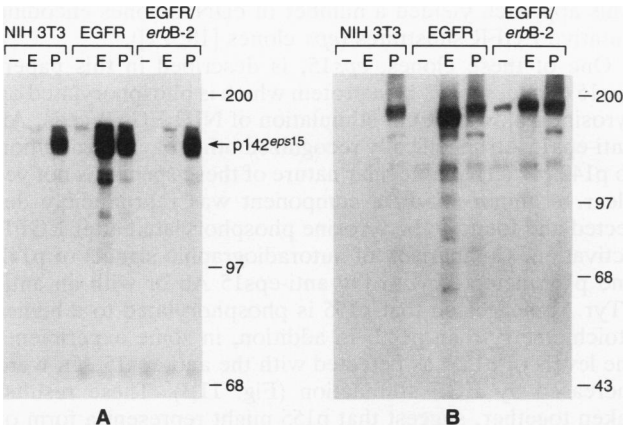

FIG. 9. Tyrosine phosphorylation of the *eps*15 gene product(s) by EGFR, *erb*B-2, and PDGFR kinases. Normal NIH 3T3 cells or NIH 3T3 transfected with the wild-type EGFR (11, 20) or the EGFR/*erb*B-2 chimera (20, 39) were either mock treated (lanes −) or treated with EGF (100 ng/ml; 17 nM) (lanes E) or PDGF-BB (100 ng/ml; ~3.2 nM) (lanes P) for 10 min at 37°C, and total cellular lysates were prepared as described in Materials and Methods. (A) Total cellular proteins (2 mg) were immunoprecipitated with the anti-pTyr Ab and analyzed in immunoblot with anti-eps15 Ab. (B) Total cellular proteins (100 μg) were directly analyzed in immunoblot with the anti-pTyr Ab. Molecular mass markers are indicated in kilodaltons. The properties of the EGFR and EGFR/*erb*B-2 expressed in the NIH 3T3 transfectants have been described previously (11, 20, 39, 54, 55). For the experiments described in this paper, transfectants expressing comparable levels of EGFR or EGFR/*erb*B-2 (3×10^5 to 5×10^5 receptors per cell) were selected. See Fig. 10 for details of the molecular constructions and ^{125}I-EGF saturation-binding assays of the transfectants used.

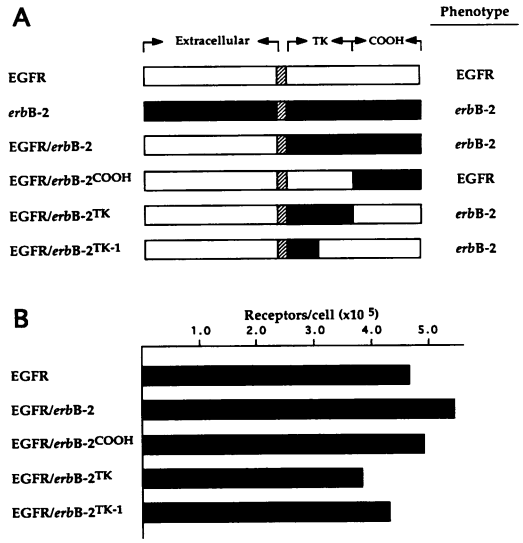

FIG. 10. Structure, biological activity, and levels of expression of EGFR/*erb*B-2 chimeric molecules. (A) Structure of the chimeric molecules used to map the region of EGFR responsible for efficient phosphorylation of eps15. The chimeric vectors used in the experiments shown all contained a transmembrane region from gp185^{erbB-2}, but similar results were obtained when using chimerae bearing the EGFR transmembrane. The biological phenotype of the various constructs, assayed by adoptive expression in NIH 3T3 or 32D cells, is also indicated. An EGFR phenotype is defined by strong mitogenic coupling in 32D and a weaker ability to transform NIH 3T3 cells, and an *erb*B-2 phenotype is characterized by the opposite behavior (9, 15, 55). (B) ^{125}I-EGF saturation binding of transfectants expressing either the wild-type EGFR or various chimeric constructs. The binding characteristics of the various transfectants have been previously reported (19, 54, 55); in particular, we showed that the chimeric molecules bind EGF with affinities (two classes of receptors) comparable to those for the EGFR. For the experiments described in this paper, ^{125}I-EGF saturation-binding assays were performed on several mass populations of each transfectant. The mass populations showing the closest numbers of receptors (3×10^5 to 5×10^5 receptors per cell, as shown in the figure) were selected for further studies.

~150 amino acids of the intracellular region of gp185^{erbB-2} for the analogous region of EGFR (juxtamembrane or TK-1 domain) was alone sufficient to decrease the ability of the chimeric EGFR/*erb*B-2^{TK1} receptor to phosphorylate eps15 (Fig. 11A). These differences were not due to different levels of expression of eps15 in the various transfectants (Fig. 11B). We concluded, therefore, that the juxtamembrane (or TK-1) region of the EGFR and *erb*B-2 is important in determining the relative efficiency of these two receptors at phosphorylating eps15. At present, however, we do not know whether the juxtamembrane regions affect eps15 phosphorylation by direct interaction or by a conformational effect on other regions of the receptor molecules.

We have previously demonstrated that wild-type EGFR and *erb*B-2 and the above-mentioned chimeric molecules display distinct mitogenic properties when expressed in different target cells (9, 15, 55). In particular, by adoptive expression of either EGFR or gp185^{erbB-2} in NIH 3T3 fibroblasts and 32D hematopoietic cells, we were able to identify an EGFR phenotype, defined by strong mitogenic coupling in 32D and weaker ability to transform NIH 3T3 cells, and an *erb*B-2 phenotype characterized by the opposite behavior (Fig. 10A) (9, 15). The use of the chimeric EGFR/*erb*B-2^{COOH}, EGFR/*erb*B-2^{TK}, and EGFR/*erb*B-2^{TK-1} receptors also allowed us to identify the TK-1 region as responsible for determining the biological phenotype (Fig. 10A) (9, 16, 55). It was therefore of interest that the ability of EGFR, *erb*B-2, and the chimeric receptors to phosphorylate eps15 correlated with their relative biological activities (compare Fig. 10A and 11A).

Overexpression of eps15 transforms NIH 3T3 cells. The pCEV-*eps*15 clone (full-length *eps*15 clone) was originally obtained from an expression library from mouse keratinocytes in which cDNA inserts were cloned under the transcriptional control of the Moloney murine leukemia virus long terminal repeat (45) (Fig. 12A). We therefore transfected the pCEV-*eps*15 cDNA, which also contained the *neo* selectable marker conferring resistance to G418, into NIH 3T3 cells to test its biological activity. pCEV-*eps*15 displayed a low but reproducible transforming activity of about 5 to 10 FFU/pmol of DNA, whereas a control pCEV plasmid did not exhibit any transforming ability (Table 1). In comparison, a eukaryotic expression vector for EGFR induced transformed foci with an efficiency of about 100 FFU/pmol of DNA, in the presence of EGF (Table 1). Similarly a v-*erb*B construct, which encodes an activated form of the avian EGFR, induced about 200 foci per pmol of transfected DNA. Conversely, a long terminal repeat (LTR)-based expression vector for PLC-γ, a known substrate of the EGFR kinase, was unable to transform NIH 3T3 cells in repeated experiments (Table 1).

The results of the transfection assay were paralleled by those obtained in an anchorage-independent test in soft agar. In this assay, NIH *eps*15 transfectants exhibited a low but

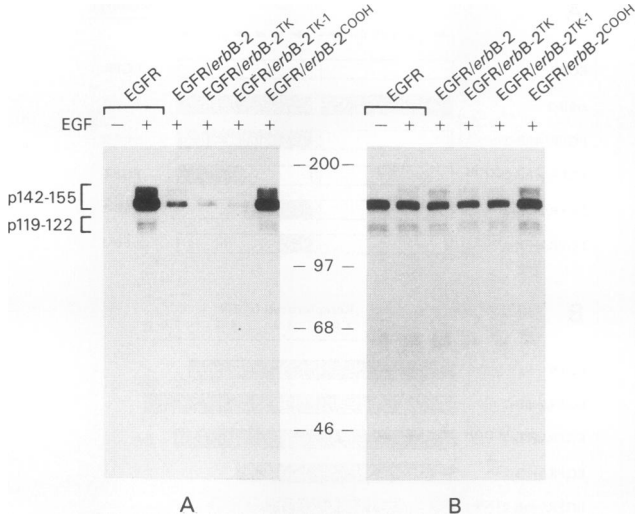

FIG. 11. Mapping of the regions of EGFR and *erb*B-2 involved in determining the differential phosphorylation of eps15. The NIH 3T3 transfectants characterized in Fig. 10 and expressing either the wild-type EGFR or the various chimeric constructs were either mock treated (lanes −) or treated with EGF (100 ng/ml; 17 mM) for 10 min at 37°C. (A) Total cellular proteins (2 mg) were immunoprecipitated with anti-pTyr and analyzed by immunoblot with the anti-eps15 Ab. (B) Total cellular proteins (100 μg) were directly analyzed by immunoblot with the anti-eps15 Ab. Molecular mass markers are indicated in kilodaltons.

reproducible growth efficiency of about 1 to 2%, whereas no anchorage-independent growth was detected in PLC-γ transfectants or in NIH 3T3 cells transfected with control pCEV vector (Table 1). EGFR and v-*erb*B transfectants exhibited about 10 to 20% clonogenic efficiency in soft agar (Table 1).

To further investigate the mechanisms of *eps*15-induced transformation, individual transformed foci were picked and selected in G418-containing medium for biological and biochemical analysis (see Materials and Methods for details). Mass populations were also obtained by selecting in G418-containing medium NIH 3T3 cells transfected with 1 μg of pCEV-*eps*15. As shown in Fig. 12B, two different mass populations of NIH *eps*15 cells displayed a 2- to 3-fold increased content of $p142^{eps15}$, whereas two representative foci overexpressed $p142^{eps}15$ in excess of 20-fold. The levels of *eps*15 expression correlated with the potency of the transformed phenotype. The NIH *eps*15 mass populations, in fact, exhibited low efficiency of colony formation in agar (Fig. 12C); however, the efficiency was significantly higher than that of NIH pCEV control cells (Fig. 12C). Conversely, the two transformed foci displayed strong ability to grow under anchorage-independent conditions (Fig. 12C). The high clonogenic ability of these last two populations also correlated with their clearly transformed morphology (Fig. 12D), whereas the NIH-*eps*15 mass populations showed more subtle morphological changes when compared with NIH pCEV controls (Fig. 12D). On the basis of all these results, we concluded that overexpression of *eps*15, above some critical threshold, is sufficient to transform NIH 3T3 fibroblasts.

DISCUSSION

A strategy for expression cloning of substrates for RTKs was used to analyze EGFR-activated signaling pathways. This approach yielded a number of cDNA clones encoding putative EGFR substrates (*eps* clones [18, 21]).

One of these clones, *eps*15, is described in this paper. *eps*15 encodes a 142-kDa protein which is phosphorylated on tyrosine following EGF stimulation of NIH EGFR cells. An anti-eps15 Ab specifically recognized other bands in addition to $p142^{eps15}$. The molecular nature of these species is not yet clear. A minor 155-kDa component was reproducibly detected and found to be tyrosine phosphorylated after EGFR activation. Comparison of autoradiographic signals of p142 and p155 detected with the anti-eps15 Ab or with an anti-pTyr Ab suggested that p155 is phosphorylated to a higher stoichiometry than p142. In addition, in some experiments the levels of p155, as detected with the anti-eps15 Ab, were increased by EGF stimulation (Fig. 11B). These results, taken together, suggest that p155 might represent a form of p142 modified by EGF-induced posttranslational modifications, possibly including tyrosine phosphorylation. A second doublet of 119 and 122 kDa was also detected. A longer exposure of the autoradiogram in Fig. 3C revealed that these species also contain pTyr after EGF stimulation (see also Fig. 11A). It is unlikely that p119-122 represents a precursor or degradation product of p142. In fact, in NIH 3T3 cells transfected with pCEV-*eps*15 and overexpressing $p142^{eps15}$ in excess of 20-fold, increased levels of these proteins were not detected. The p119-122 component might represent, therefore, either the product of an alternative splicing event, originating perhaps from the 6.0-kb mRNA, or a related species.

Computer-assisted analysis of the predicted *eps*15 gene product allowed its division into three structural domains. Some of the features of these regions prompt the speculation that they might actually encode distinct functional domains. Domain I presents signatures suggestive of a regulatory domain, including a putative tyrosine phosphorylation site and calcium-binding domains of the EF-hand type.

Domain II is most probably a coiled-coil structure. In this domain significant homology is detected between eps15 and several proteins with rod-like structures, including myosin heavy chains, desmoplakins, involucrins, keratins, and the *Saccharomyces cerevisiae* USO1 protein. The USO1 protein, which is involved in intracellular transport (48), further shares with eps15 the presence of EF-hand calcium-binding domains (48). The presence of a coiled-coil structure is characteristic of cytoskeleton-related proteins and conditions the formation of filamentous structures (7). Domain II might therefore be important in determining $p142^{eps15}$ localization and its interactions with other proteins.

Domain III is characterized by the DPF motif. Data bank searches produced only one protein containing more than one DPF repeats, i.e., the *Caenorhabditis elegans* protein twitchin (4). However, this similarity is most probably fortuitous. Twitchin is, in fact, composed of a monotonous repetition of two motifs. Motif I is ~100 amino acids long and is repeated 31 times (4): the DPF repeat is present in only 4 of 31 copies of motif I of twitchin. There is reason, however, to speculate that domain III might encode an effector domain in $p142^{eps15}$. A DPF motif is well conserved, as part of a consensus sequence, in a heterogeneous class of protein displaying methyltransferase activity (31). The hypothesis has been put forward that the DPF-containing consensus sequence might be part of the recognition sequence for *S*-adenosylmethionine, the methyl group donor in the methyltransferase reaction (31). The issue of whether $p142^{eps15}$ is endowed with methylase activity and, if so,

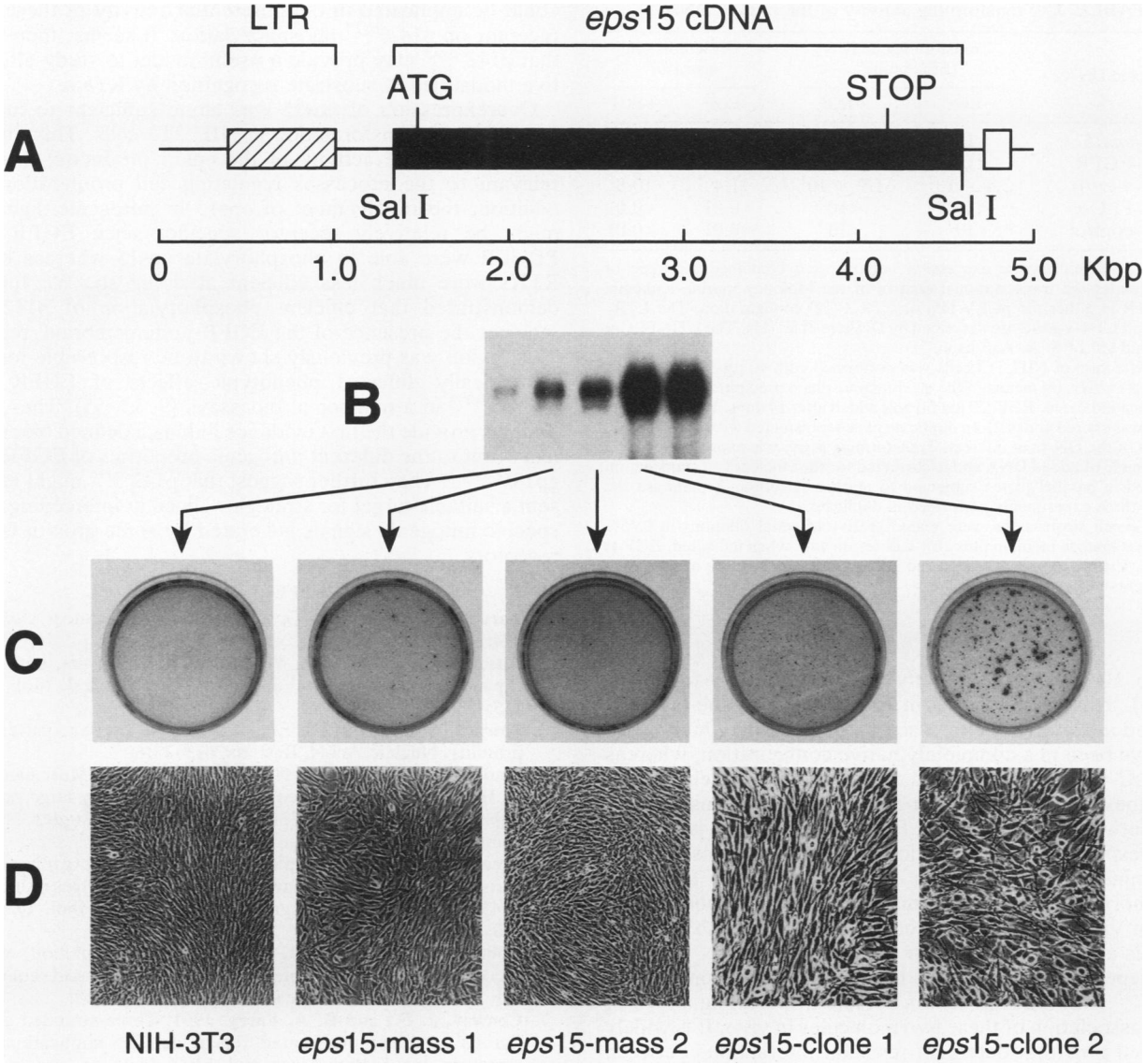

FIG. 12. Transformation of NIH 3T3 cells by an *eps*15 eukaryotic expression vector. (A) Structure of the pCEV-*eps*15 expression vector. The *eps*15 cDNA is indicated by a solid box. The dashed and empty boxes represent the Moloney murine leukemia virus LTR promoter and the simian virus 40 polyadenylation signal, respectively (for details of the pCEV vector, see reference 45). (B to D) The pCEV-*eps*15 or a pCEV control vector were transfected in NIH 3T3 cells at a concentration of 1 μg, as indicated in Materials and Methods. Mass populations of cells transfected with pCEV (NIH 3T3) or pCEV-*eps*15 (*eps*15-mass 1 and *eps*15-mass 2) were then obtained by selection in G418. From nonselected plates, a number of morphologically transformed foci were also picked and then selected in G418: two representative foci (*eps*15-clone 1 and *eps*15-clone 2) are shown. Panel B shows levels of expression of *eps*15 product(s). Total cellular proteins (100 μg) from the above indicated mass populations and foci were analyzed in immunoblot with the anti-eps15 Ab. Lanes (left to right): NIH 3T3 control, *eps*15-mass 1, *eps*15-mass 2, *eps*15-clone 1, *eps*15-clone 2. They correspond to the cell lines shown in panels C and D. Panel C shows anchorage-independent growth of the *eps*15-overexpressing mass populations and foci. The soft agar assay was performed as described in Materials and Methods. Plates were stained with *p*-iodonitrotetrazolium violet before photography. Panel D shows morphology of NIH 3T3 transfected with pCEV (NIH 3T3) or with pCEV-*eps*15 (mass populations and foci).

which is its specificity therefore appears worthy of further investigation.

On the basis of our results, we cannot definitively conclude that $p142^{eps15}$ is a direct substrate for the EGFR; the alternative possibility is that it is phosphorylated by a secondary kinase activated by the EGFR. We want to point out, however, that eps15 phosphorylation was detectable in vivo as early as 15 s after EGF stimulation and exhibited time-dependent kinetics resembling those observed for the phosphorylation of authentic substrates, such as PLC-γ. In addition, eps15 phosphorylation in vivo occurred at physiological levels of EGFR activation. Finally, under the conditions of an immunocomplex kinase assay, the EGFR was able to directly phosphorylated purified eps15 in vitro. All this evidence militates in favor of the possibility of direct phosphorylation of eps15 by EGFR. It should be pointed out, however, that under the conditions of an immunocomplex kinase assay, eps15 was phosphorylated by the EGFR

TABLE 1. Transforming activity of the *eps*15 cDNA

Transfected DNA[a]	Transforming activity (FFU/pmol)[b]		Growth in soft agar (%)[c]	
	−EGF	+EGF	−EGF	+EGF
LTR–*eps*15	10^1	10^1	1.5	2.0
LTR–EGFR	$<10^0$	1.5×10^2	0.1	17.8
LTR–v-*erb*B	2.4×10^2	1.9×10^2	11.4	10.8
LTR–PLC-γ	$<10^0$	$<10^0$	<0.01	<0.01
LTR–control	$<10^0$	$<10^0$	<0.01	<0.01

[a] All of the eukaryotic expression vectors used contained the gene of interest under the transcriptional control of the Moloney murine leukemia virus LTR in either the pCEV (45) or LTR-2 (12) configuration. The LTR–EGFR and LTR–v-*erb*B are described by Di Fiore et al. (11). The LTR–PLC-γ was a kind gift of S. A. Aaronson.

[b] Transfection of NIH 3T3 cells was performed with 40 μg of calf thymus DNA as a carrier, by means of the calcium phosphate precipitation technique (65). When indicated, EGF (20 ng/ml) was added after 14 days. Focus-forming activity was scored at day 21 on duplicate plates transfected with serial 10-fold dilutions of the DNAs of interest. Transforming activity is expressed in FFU per picomole of added DNA and is corrected for the efficiency of transfection calculated in parallel plates subjected to marker selection. Results are the mean of three experiments performed in duplicate.

[c] Single-cell suspensions were plated at 10-fold serial dilutions in 0.45% SeaPlaque agarose medium plus 10% calf serum and, when indicated, EGF at 20 ng/ml. Visible colonies were scored at day 14. Results are the mean of two experiments performed in duplicate.

~5- to 10-fold less efficiently than was PLC-γ (data not shown). This difference might be attributed to the fact that we used a bacterially expressed eps15 protein, which might not have been in a completely native configuration, whereas the PLC-γ used was purified from mammalian cells. However, these differences might also reflect an intrinsic difference between the abilities of EGFR to phosphorylate eps15 with respect to an authentic substrate, such as PLC-γ. Determination of the K_m for ATP and substrate for eps15 phosphorylation in vitro and mapping of the phosphorylation sites in vivo and in vitro should help to establish whether eps15 is a direct substrate for the EGFR kinase.

In repeated experiments, no coimmunoprecipitation of p142^{eps15} with the EGFR was detected, indicating a lack of stable association of these two molecules in vivo. It is widely accepted now that detergent-resistant interactions between RTKs and some of their substrates are made possible by binding of specialized regions of substrate molecules, known as SH2 domains, to pTyr motifs present in RTKs (reviewed in reference 32). In this regard, we note that the *eps*15 cDNA predicts the synthesis of a protein lacking SH2 domains. However, a stable association between RTKs and their substrates is not obligatory. Ezrin, for example, does not stably associate with the EGFR but appears to be a good substrate for its kinase (5, 24). There is additional reason to believe that the SH2-pTyr interactions are not the only ones responsible for receptor/substrate recognition. The cell-specific signaling differences between EGFR and *erb*B-2, for example, are not determined by their COOH-terminal domains (15), which contain all of the autophosphorylation sites (25), but, rather, by their juxtamembrane regions (15, 55). In addition, a deletion mutant with a mutation in the juxtamembrane region of the EGFR displayed greatly decreased mitogenic potency in the absence of any alteration of intrinsic kinase activity or ability to interact with and phosphorylate SH2-containing substrates, such as PLC-γ (55). Thus, other receptor-substrate interactions, possibly of a weaker type, might exist. In this respect, it is interesting that the juxtamembrane region of the EGFR and *erb*B-2 could be implicated in the differential activity of these two receptor on p142^{eps15} phosphorylation. It seems, therefore, that p142^{eps15} may provide a useful model to study alternative modalities of substrate recognition by RTKs.

Overexpression of *eps*15 was alone sufficient to induce low levels of transformation in NIH 3T3 cells. This finding suggests that the activity of the eps15 product(s) may be relevant to the processes regulating cell proliferation. In addition, the involvement of eps15 in mitogenic signaling might be relatively receptor specific, since EGFR and PDGFR were able to phosphorylate eps15 whereas other RTKs were much less efficient at doing so. We further demonstrated that efficient phosphorylation of p142^{eps15} requires the presence of the EGFR juxtamembrane region. This region was previously shown to be responsible for the dramatically different phenotypic effects of EGFR and gp185^{erbB-2} in a number of bioassays (9, 15, 55). Thus, our findings provide the first evidence linking a defined biochemical event to the different mitogenic properties of EGFR and gp185^{erbB-2}. They further suggest that p142^{eps15} might represent a suitable target for strategies aimed at interceding with specific mitogenic signals generated by some growth factor receptors.

REFERENCES

1. **Aaronson, S. A.** 1991. Growth factors and cancer. Science **254**:1146–1153.
2. **Altschul, S. F., W. Gish, W. Miller, E. W. Myers, and D. J. Lipman.** 1990. Basic local alignment search tool. J. Mol. Biol. **215**:403–410.
3. **Bairoch, A.** 1992. PROSITE: a dictionary of sites and patterns in proteins. Nucleic Acids. Res. **20**:2013–2018.
4. **Benian, G. M., J. E. Kiff, N. Neckelmann, D. G. Moerman, and R. H. Waterston.** 1989. Sequence of an unusually large protein implicated in regulation of myosin activity in *C. elegans*. Nature (London) **342**:45–50.
5. **Bretscher, A.** 1989. Rapid phosphorylation and reorganization of ezrin and spectrin accompany morphological changes induces in A-431 cells by epidermal growth factor. J. Cell Biol. **108**:921–930.
6. **Chou, P. Y., and G. D. Fasman.** 1978. Prediction of the secondary structure of proteins from their amino acid sequence. Adv. Enzymol. Relat. Areas Mol. Biol. **47**:45–148.
7. **Conway, J. F., and D. A. Parry.** 1991. Three-stranded alpha-fibrous proteins: the heptad repeat and its implications for structure. Int. J. Biol. Macromol. **13**:14–16.
8. **Coughlin, S. R., J. A. Escobedo, and L. T. Williams.** 1989. Role of phosphatidylinositol kinase in PDGF receptor signal transduction. Science **243**:1191–1194.
9. **Di Fiore, P. P., K. Helin, M. H. Kraus, J. H. Pierce, J. Artrip, O. Segatto, and D. P. Bottaro.** 1992. A single amino acid substitution is sufficient to modify the mitogenic properties of the epidermal growth factor receptor to resemble that of gp185^{erbB-2}. EMBO J. **11**:3927–3933.
10. **Di Fiore, P. P., and M. H. Kraus.** 1992. Mechanisms involving an expanding erbB/EGF receptor family of tyrosine kinases in human neoplasia, p. 139–160. *In* R. B. Dickson and M. E. Lippman (ed.), Genes, oncogenes and hormones: advances in cellular and molecular biology of breast cancer. Kluwer Academic Publishers, Boston.
11. **Di Fiore, P. P., J. H. Pierce, T. P. Fleming, R. Hazan, A. Ullrich, C. R. King, J. Schlessinger, and S. A. Aaronson.** 1987. Overexpression of the human EGF receptor confers an EGF-dependent transformed phenotype to NIH 3T3 cells. Cell **51**:1063–1070.
12. **Di Fiore, P. P., J. H. Pierce, M. H. Kraus, O. Segatto, C. R. King, and S. A. Aaronson.** 1987. erbB-2 is a potent oncogene when overexpressed in NIH-3T3 cells. Science **237**:178–182.
13. **Di Fiore, P. P., O. Segatto, and S. A. Aaronson.** 1991. Cloning, expression and biological effects of *erb*B-2/*neu* gene in mammalian cells. Methods Enzymol. **198**:272–277.
14. **Di Fiore, P. P., O. Segatto, F. Lonardo, F. Fazioli, J. H. Pierce,**

and S. A. Aaronson. 1990. The carboxy-terminal domains of *erb*B-2 and epidermal growth factor receptor exert different regulatory effects on intrinsic receptor tyrosine kinase function and transforming activity. Mol. Cell. Biol. **10**:2749–2756.

15. **Di Fiore, P. P., O. Segatto, W. G. Taylor, S. A. Aaronson, and J. H. Pierce.** 1990. EGF receptor and *erb*B-2 tyrosine kinase domains confer cell specificity for mitogenic signaling. Science **248**:79–83.
16. **Ellis, C., M. Moran, F. McCormick, and T. Pawson.** 1990. Phosphorylation of GAP and GAP-associated proteins by transforming and mitogenic tyrosine kinases. Nature (London) **343**: 377–381.
17. **Escobedo, J. A., S. Navankasattusas, W. M. Kavanaugh, D. Milfay, V. A. Fried, and L. T. Williams.** 1991. cDNA cloning of a novel 85 kd protein that has SH2 domains and regulates binding of P13-kinase to the PDGF beta-receptor. Cell **65**:75–82.
18. **Fazioli, F., D. P. Bottaro, L. Minichiello, A. Auricchio, W. T. Wong, O. Segatto, and P. P. Di Fiore.** 1992. Identification and biochemical characterization of novel putative substrates for the epidermal growth factor receptor kinase. J. Biol. Chem. **267**: 5155–5161.
19. **Fazioli, F., and P. P. Di Fiore.** Unpublished observations.
20. **Fazioli, F., U.-H. Kim, S. G. Rhee, C. J. Molloy, O. Segatto, and P. P. Di Fiore.** 1991. The *erb*B-2 mitogenic signaling pathway: tyrosine phosphorylation of phospholipase C-γ and GTPase-activating protein does not correlate with *erb*B-2 mitogenic potency. Mol. Cell. Biol. **11**:2040–2048.
21. **Fazioli, F., W. T. Wong, S. J. Ullrich, K. Sakaguchi, E. Appella, and P. P. Di Fiore.** 1993. The ezrin-like family of tyrosine kinase substrates: receptor-specific pattern of phosphorylation and relationship to malignant transformation. Oncogene **8**:1335–1345.
22. **Fukui, Y., and H. Hanafusa.** 1989. Phosphatidylinositol kinase activity associates with viral $p60^{src}$ protein. Mol. Cell. Biol. **9**:1651–1658.
23. **Gould, K., and T. Hunter.** 1988. Platelet-derived growth factor induces multisite phosphorylation of $pp60^{c\text{-}src}$ and increases its protein-tyrosine kinase activity. Mol. Cell. Biol. **8**:3345–3356.
24. **Gould, K. L., J. A. Cooper, A. Bretscher, and T. Hunter.** 1986. The protein-tyrosine kinase substrate p81, is homologous to a chicken microvillar core protein. J. Cell Biol. **102**:660–669.
25. **Hazan, R., B. Margolis, M. Dombalagian, A. Ullrich, A. Zilberstein, and J. Schlessinger.** 1990. Identification of autophosphorylation sites of HER2/neu. Cell Growth Differ. **1**:3–7.
26. **Heizmann, C. W., and W. Hunziker.** 1991. Intracellular calcium-binding proteins: more sites than insights. Trends Biochem. Sci. **16**:98–103.
27. **Hunter, T.** 1982. Synthetic peptide substrates for a tyrosine protein kinase. J. Biol. Chem. **257**:4843–4848.
28. **Kaplan, D. R., D. K. Morrison, G. Wong, F. McCormick, and L. T. Williams.** 1990. PDGF beta-receptor stimulates tyrosine phosphorylation of GAP and association of GAP with a signaling complex. Cell **61**:125–133.
29. **Kazlauskas, A., and J. A. Cooper.** 1989. Autophosphorylation of the PDGF receptor in the kinase insert region regulates interactions with cell proteins. Cell **58**:1121–1123.
30. **Kazlauskas, A., C. Ellis, T. Pawson, and J. A. Cooper.** 1990. Binding of GAP to activated PDGF receptors. Science **247**: 1578–1581.
31. **Klimasauskas, S., A. Timinskas, S. Menkevicius, D. Butkiene, V. Butkus, and A. Janulaitis.** 1989. Sequence motifs characteristic of DNA [cytosine-N4] methyltransferases: similarity to adenine and cytosine-C5 DNA-methylases. Nucleic Acids Res. **17**:9823–9832.
32. **Koch, C. A., D. Anderson, M. F. Moran, C. Ellis, and T. Pawson.** 1991. SH2 and SH3 domains: elements that control interactions of cytoplasmic signaling proteins. Science **252**:668–674.
33. **Koerner, T. J., J. E. Hill, A. M. Myers, and A. Tzagoloff.** 1991. High-expression vectors with multiple cloning sites for construction of trpE fusion genes: pATH vectors. Methods Enzymol. **194**:477–490.
34. **Kozak, M.** 1989. The scanning model for translation: an update. J. Cell Biol. **108**:229–241.
35. **Kypta, R. M., Y. Goldberg, E. T. Ulug, and S. A. Courtneidge.** 1990. Association between the PDGF receptor and members of the src family of tyrosine kinases. Cell **62**:481–492.
36. **Kyte, J., and R. F. Doolittle.** 1982. A simple method for displaying the hydropathic character of a protein. J. Mol. Biol. **157**:105–132.
37. **Lee, J., T. J. Dull, I. Lax, J. Schlessinger, and A. Ullrich.** 1989. HER2 cytoplasmic domain generates normal mitogenic and transforming signals in a chimeric receptor. EMBO J. **8**:167–173.
38. **Lehvaslaiho, H., L. Lehtola, L. Sistonen, and K. Alitalo.** 1989. A chimeric EGF-R-neu proto-oncogene allows EGF to regulate neu tyrosine kinase and cell transformation. EMBO J. **8**:159–166.
39. **Lonardo, F., E. Di Marco, C. R. King, J. H. Pierce, O. Segatto, S. A. Aaronson, and P. P. Di Fiore.** 1990. The normal *erb*B-2 product is an atypical receptor-like tyrosine kinase with constitutive activity in the absence of ligand. New Biol. **2**:992–1003.
40. **McLachlan, A. D., and J. Karn.** 1983. Periodic features in the amino acid sequence of nematode myosin rod. J. Mol. Biol. **164**:605–626.
41. **Majerus, P. W., T. S. Ross, T. W. Cunningham, K. K. Caldwell, A. B. Jefferson, and V. S. Bansal.** 1990. Recent insights in phosphatidylinositol signaling. Cell **63**:459–465.
42. **Margolis, B., S. G. Rhee, S. Felder, M. Mervice, R. Lyall, A. Levitzki, A. Ullrich, A. Zilberstein, and J. Schlessinger.** 1989. EGF induces tyrosine phosphorylation of phospholipase C-II: a potential mechanism for EGF receptor signaling. Cell **57**:1101–1107.
43. **Margolis, B., A. Zilberstein, C. Franks, S. Felder, S. Kremer, A. Ullrich, S. G. Rhee, K. Skorecki, and J. Schlessinger.** 1990. Effect of phospholipase C-gamma overexpression on PDGF-induced second messengers and mitogenesis. Science **248**:607–610.
44. **Meisenhelder, J., P.-G. Suh, S. G. Rhee, and T. Hunter.** 1989. Phospholipase C-gamma is a substrate for the PDGF and EGF receptor protein-tyrosine kinases in vivo and in vitro. Cell **57**:1109–1122.
45. **Miki, T., T. P. Fleming, D. P. Bottaro, J. S. Rubin, D. Ron, and S. A. Aaronson.** 1991. Expression cDNA cloning of the KGF receptor by creation of a transforming autocrine loop. Science **251**:72–75.
46. **Mohammadi, M., C. A. Dionne, W. Li, N. Li, T. Spivak, A. M. Honegger, M. Jaye, and J. Schlessinger.** 1992. Point mutation in FGF receptor eliminates phosphatidylinositol hydrolysis without affecting mitogenesis. Nature (London) **358**:681–684.
47. **Molloy, C. J., D. P. Bottaro, T. P. Fleming, M. S. Marshall, J. B. Gibbs, and S. A. Aaronson.** 1989. PDGF induction of tyrosine phosphorylation of GTPase activating protein. Nature (London) **342**:711–714.
48. **Nakajima, H., A. Hirata, Y. Ogawa, T. Yonehara, K. Yoda, and M. Yamasaki.** 1991. A cytoskeleton-related gene, usol, is required for intracellular protein transport in Saccharomyces cerevisiae. J. Cell Biol. **113**:245–260.
49. **Otsu, M., I. Hiles, M. Gout, M. J. Fry, F. Ruiz-Larrea, G. Panayatou, A. Thompson, R. Dhand, J. Hsuan, N. Totty, A. D. Smith, S. J. Morgan, S. A. Courtneidge, D. J. Parker, and M. D. Waterfield.** 1991. Characterization of two 85 kd proteins that associate with receptor tyrosine kinases, middle-T/$pp60^{c\text{-}src}$ complexes, and PI3-kinase. Cell **65**:91–104.
50. **Pelicci, G., L. Lanfrancone, F. Grignani, J. McGlade, F. Cavallo, G. Forni, I. Nicoletti, F. Grignani, T. Pawson, and P. G. Pelicci.** 1992. A novel transforming protein (SHC) with an SH2 domain is implicated in mitogenic signal transduction. Cell **70**:93–104.
51. **Peters, K. G., J. Marie, E. Wilson, H. E. Ives, J. Escobedo, M. Del Rosario, D. Mirda, and L. T. Williams.** 1992. Point mutation of an FGF receptor abolishes phosphatidylinositol turnover and Ca^{2+} flux but not mitogenesis. Nature (London) **358**:678–681.
52. **Ruderman, N. B., R. Kapeller, M. F. White, and L. C. Cantley.** 1990. Activation of phosphatidylinositol 3-kinase by insulin. Proc. Natl. Acad. Sci. USA **87**:1411–1415.

53. **Sambrook, J., E. F. Fritsch, and T. Maniatis.** 1989. Molecular cloning: a laboratory manual, 2nd ed. Cold Spring Harbor Laboratory Press, Cold Spring Harbor, N.Y.
54. **Segatto, O., F. Lonardo, K. Helin, D. Wexler, F. Fazioli, S. G. Rhee, and P. P. Di Fiore.** 1992. *erb*B-2 autophosphorylation is required for mitogenic action and high-affinity substrate coupling. Oncogene **7**:1339–1346.
55. **Segatto, O., F. Lonardo, D. Wexler, F. Fazioli, J. H. Pierce, D. P. Bottaro, M. F. White, and P. P. Di Fiore.** 1991. The juxtamembrane regions of the epidermal growth factor receptor and gp185^{erbB-2} determine the specificity of signal transduction. Mol. Cell. Biol. **11**:3191–3202.
56. **Settleman, J., V. Narasimhan, L. C. Foster, and R. A. Weinberg.** 1992. Molecular cloning of cDNAs encoding the GAP-associated protein p190: implications for a signaling pathway from *ras* to the nucleus. Cell **69**:539–549.
57. **Skolnik, E. Y., B. Margolis, M. Mohammadi, E. Lowenstein, R. Fischer, A. Drepps, A. Ullrich, and J. Schlessinger.** 1991. Cloning of PI3 kinase-associated p85 utilizing a novel method for expression/cloning of target proteins for receptor tyrosine kinases. Cell **65**:83–90.
58. **Smith, M. R., S. H. Ryu, P. G. Suh, S. G. Rhee, and H. F. Kung.** 1989. S-phase induction and transformation of quiescent NIH 3T3 cells by microinjection of phospholipase C. Proc. Natl. Acad. Sci. USA **86**:3659–3663.
59. **Southern, P. J., and P. Berg.** 1982. Transformation of mammalian cells to antibiotic resistance with a bacterial gene under control of the SV40 early region promoter. J. Mol. Appl. Genet. **1**:327–341.
60. **Ullrich, A., and J. Schlessinger.** 1990. Signal transduction by receptors with tyrosine kinase activity. Cell **61**:203–212.
61. **Varticovski, L., B. Druker, D. Morrison, L. Cantley, and T. M. Roberts.** 1989. The colony stimulating factor-1 receptor associates with and activates phosphatidylinositol-3 kinase. Nature (London) **342**:699–702.
62. **Wahl, M. I., N. E. Olashaw, S. Nishibe, S. G. Rhee, W. J. Pledger, and G. Carpenter.** 1989. Platelet-derived growth factor induces rapid and sustained tyrosine phosphorylation of phospholipase C-γ in quiescent BALB/c 3T3 cells. Mol. Cell. Biol. **9**:2934–2943.
63. **Weissman, B. E., and S. A. Aaronson.** 1983. BALB and Kirsten murine sarcoma viruses alter growth and differentiation of EGF-dependent BALB/c mouse epidermal keratinocyte lines. Cell **32**:599–606.
64. **Whitman, M., and L. Cantley.** 1989. Phosphoinositide metabolism and the control of cell proliferation. Biochim. Biophys. Acta **948**:327–344.
65. **Wigler, M., S. Silverstein, L. S. Lee, A. Pellicer, Y. Cheng, and R. Axel.** 1977. Transfer of purified herpes virus thymidine kinase gene to cultured mouse cells. Cell **11**:223–232.
66. **Wong, G., O. Müller, R. Clark, L. Conroy, M. F. Moran, P. Polakis, and F. McCormick.** 1992. Molecular cloning and nucleic acid binding properties of the GAP-associated tyrosine phosphoprotein p62. Cell **69**:551–558.
67. **Yu, J. C., M. A. Heidaran, J. H. Pierce, J. S. Gutkind, D. Lombardi, M. Ruggiero, and S. A. Aaronson.** 1991. Tyrosine mutations within the alpha platelet-derived growth factor receptor kinase insert domain abrogate receptor-associated phosphatidylinositol-3 kinase activity without affecting mitogenic or chemotactic signal transduction. Mol. Cell. Biol. **11**:3780–3785.